HHS Public Access

Author manuscript

J Hepatol. Author manuscript; available in PMC 2022 April 01.

Published in final edited form as:

J Hepatol. 2022 April ; 76(4): 850–861. doi:10.1016/j.jhep.2021.12.019.

Histone acetylation of bile acid transporter genes plays a critical role in cirrhosis

Amanda Garrido[1,8], **Eunjeong Kim**[1,8], **Ana Teijeiro**[1], **Paula Sánchez Sánchez**[1], **Rosa Gallo**[1], **Ajay Nair**[2], **Maria Matamala**[1], **Cristian Perna**[3], **Guillermo Pablo Vicent**[4], **Javier Muñoz**[5], **Ramon Campos-Olivas**[6], **Johannes C. Melms**[7], **Benjamin Izar**[7], **Robert Friedrich Schwabe**[2], **Nabil Djouder**[1,*]

[1]Molecular Oncology Programme, Growth Factors, Nutrients and Cancer Group, Centro Nacional Investigaciones Oncológicas (CNIO), Madrid, 28029, Spain,

[2]Department of Medicine, Columbia University, New York, NY 10032, USA.

[3]Department of Pathology, Hospital Universitario Ramón y Cajal (IRYCIS), Madrid, 28034, Spain,

[4]Molecular Biology Institute of Barcelona, Consejo Superior de Investigaciones Científicas (IBMB-CSIC), Barcelona, 08028, Spain,

[5]Biotechnology Programme, Proteomics Core Unit, Centro Nacional Investigaciones Oncológicas (CNIO), Madrid, 28029, Spain,

[6]Structural Biology Programme, Spectrometry and Nuclear Magnetic Resonance Unit, Centro Nacional Investigaciones Oncológicas (CNIO), Madrid, 28029, Spain.

[7]Department of Medicine, Division of Hematology and Oncology, Irving Medical Center, Columbia University, New York, NY 10032, USA.

Abstract

Background & Aims: Cirrhosis is a deadly liver disease; fibrosis being a key feature. Due to the lack of genetic animal models exhibiting clinical characteristics, molecular pathogenesis of cirrhosis has been so far poorly characterized, and treatments remain limited.

Methods: We report the first murine genetic model mimicking human cirrhosis induced by hepatocyte-specific elimination of microspherule 1 (MCRS1), a member of non-specific lethal (NSL) and INO80 chromatin-modifier complexes. Using this genetic tool with other mouse models, cell culture and human samples, combined with quantitative proteomic, single nuclear/

*Correspondence: Nabil Djouder, Tel: 0034 91 7328000 (Ext.: 3830), ndjouder@cnio.es.

[8]Equal contribution

Authors' contributions A.G., E.K. and N.D. designed the experiments and analyzed the data. A.G. performed most of the experiments associated to *Mcrs1*^{hep} mouse, *Nr1h4*^{HSC} mouse and cell experiments *in vitro*. E.K. analyzed *Mcrs1*^{hep} and *hMCRS1*^{KI} mice crossed with *Abcb4*$^{(-/-)}$ mice, performed the BDL surgeries, cell experiments *in vitro* and NTCP rescue experiment. A.T. helped with some experiments performed *in vivo* and performed the IF for epithelial-mesenchymal transition determination and co-IP experiments. P.S.S. performed DCA measurements, CD31 staining and sample preparation for flow cytometry. R.G. performed and analyzed flow cytometry experiments. A.N, R.F.S., J.C.M. and B.I. performed and analyzed the snRNA- and scRNA-seq data. C.P. analyzed mouse pathology and human samples with M.M.. G.P.V. performed ChIP assays. J.M. and R.C.O. performed iTRAQ and NMR, respectively. N.D. conceived, developed, and wrote the project, study and manuscript with A.G.. N.D. secured funding.

Conflicts of interest Authors declare no competing financial interests.

cell RNA sequencing and chromatin immunoprecipitation assays, mechanisms of cirrhosis are investigated.

Results: MCRS1 loss in mouse hepatocytes modulates the expression of bile acid (BA) transporters, with a pronounced downregulation of Na^+-taurocholate cotransporting polypeptide (NTCP), concentrating BAs in sinusoids, thereby activating hepatic stellate cells (HSCs) via nuclear farnesoid X receptor (FXR); FXR being predominantly expressed in human and mouse HSCs. Consistently, re-expression of NTCP in mice reduces cirrhosis, and genetic ablation of FXR in HSCs suppresses fibrotic marks in mice and *in vitro* cell culture. Mechanistically, deletion of a putative SANT domain from MCRS1 evicts histone deacetylase 1 (HDAC1) from its histone H3 anchoring sites, increasing histone acetylation of BA transporter genes, modulating their expression and perturbing BA flow. Accordingly, human cirrhosis displays decreased nuclear MCRS1 and NTCP expression.

Conclusions: Our data reveal a previously unrecognized function of MCRS1 as a critical histone acetylation regulator, maintaining gene expression and liver homeostasis. MCRS1 loss induces BA transporter acetylation, perturbation of BA flow, and consequently, FXR activation in HSCs. This axis represents a central and universal signaling event in liver cirrhosis, and targeting it would have significant implications for cirrhosis treatment.

Lay summary

By genetic ablation of MCRS1 in mouse hepatocytes, Garrido et al. generate the first genetic mouse model of liver cirrhosis, recapitulating human features. Garrido et al. demonstrate that the activation of the bile acid/FXR axis in liver fibroblasts is key in liver cirrhosis development.

Keywords

MCRS1; NTCP; Bile acid transporter; Bile acids; FXR; Fibroblasts; Hepatic stellate cells; Histone acetylation; Liver fibrosis; Cirrhosis

Introduction

Cirrhosis is a chronic liver disease characterized by disrupted liver architecture and zonation, along with neovascularization, and the formation of fibrotic bands and parenchymal nodules, severely impairing liver function[1]. Cirrhosis has a high risk of mortality and poor prognosis, with complications such as hepatic encephalopathy, a neuropsychiatric disorder caused by ammonia (NH_3) accumulation that eventually leads to coma[1]. Cellular mechanisms of liver fibrosis imply the transdifferentiation of HSCs into myofibroblasts that synthesize the extracellular matrix (ECM) to form fibrotic bands[1]. Although research over the last 20 years has increased our understanding of liver fibrosis, effective antifibrotic therapies are still lacking, most likely because mechanisms of HSC activation remain elusive. Murine genetic models mimicking the human disease are needed to study the processes underlying fibrogenesis, identify potential therapeutic targets, and evaluate the effectiveness of antifibrotic therapies.

Cirrhosis is mostly caused by hepatitis B and C viral infection, alcohol abuse or obesity[1]. Less frequently, cirrhosis can originate from genetic disorders[2,3] or autoimmune liver

diseases that provoke the disruption of bile ducts causing BA leakage[4]. This suggests a causal relationship between perturbation of BA flow and cirrhosis development. Primary BAs are synthesized in hepatocytes via cholesterol oxidation, mainly catalyzed by cholesterol 7 alpha-hydroxylase (CYP7A1). Then, they are conjugated with glycine or taurine before excretion to the gallbladder by the bile salt export pump (BSEP)[5,6]. Other bile components are excreted via multidrug resistance-associated protein 2/3 (human MDR3, mouse MDR2). BAs are eventually secreted into the gut to facilitate digestion of dietary lipids, where secondary BAs are formed by partial dehydroxylation catalyzed by gut bacteria. Primary and secondary BAs are efficiently recycled via the hepatic portal vein and taken up by hepatocytes via NTCP and organic anion transporting polypeptides (human OATP1B1 and OATP1B3, mouse OATP1B2)[5,6], closing the loop of the enterohepatic circulation. Excessive BAs in hepatocytes are released into the sinusoids (to eventually reach the bloodstream) thanks to heteromeric organic solute transporter (OSTα-OSTβ) and multidrug resistance-associated proteins 3 and 4 (MRP3, MRP4)[5,6]. Disruption of BA homeostasis and flow could therefore lead to the development of severe liver diseases, but mechanisms remain unknown.

Histone acetylation controls gene regulation and plays important roles in many biological processes, but it is reportedly increased in human cirrhosis[7], although no mechanism has been proposed to explain how it contributes to cirrhosis development. Several chromatin-modifier complexes participate in the tight regulation of this post-translational modification. These include the NSL complex, which contains the histone acetyltransferase males absent on the first (MOF), KAT8 regulatory NSL complex subunits 1 and 3 (KANSL1 and KANSL3), WD repeat-containing protein 5 (WDR5), and MCRS1[8]. MCRS1 is also part of the INO80 complex together with Pontin (TIP49) and Reptin (TIP48), two conserved ATPases[8]. MCRS1 might thus play a key role in modulating the cellular epigenetic landscape. Here, we show that MCRS1 is a central component of a chromatin-modifying complex, controlling expression of BA transporter genes by regulating histone acetylation in hepatocytes. Loss of MCRS1 in hepatocytes induces histone acetylation of BA transporter genes, which leads to perturbation of BA flow. Accumulation of BAs in liver sinusoids activates HSCs via FXR, promoting liver fibrosis.

Materials and methods

A full description of the materials and methods used, including generation of mouse models, can be found in the supplementary methods and CTAT table.

Results

MCRS1 Loss in Hepatocytes Promotes Cirrhosis

MCRS1 was knocked-out specifically in hepatocytes by crossing *Mcrs1* conditional knockout mice with serum albumin (SA)-creERT2 mice (Fig. S1A). CreERT2-mediated recombination was induced by dietary provision of tamoxifen to 5-week-old mice for 3 weeks, yielding $Mcrs1^{(+/+)hep}$ and $Mcrs1^{(\Delta/\Delta)hep}$ mice that were sacrificed at either 8 or 15 weeks of age (Fig. 1A and Fig. S1B). Although $Mcrs1^{(\Delta/\Delta)hep}$ mice gained weight more slowly after tamoxifen treatment than control littermates, they recovered body weight after

4 weeks, and liver to body weight ratio of 15-week-old *Mcrs1*$^{(\Delta/\Delta)hep}$ mice was identical to that of control mice (Fig. S1C, D). Histopathological analysis of livers from 8-week-old *Mcrs1*$^{(\Delta/\Delta)hep}$ mice showed that hepatocyte proliferation rate was unchanged, with cell cycle arrest in G2 phase and elevated levels of p53 and p21 (Fig. S1, E–I). Moreover, hepatic progenitor cells (HPCs) were proliferating (a measure of bile duct reaction), and fibrosis was significantly higher than in littermate controls (Fig. S1J–M). Fibrosis was accompanied by increased apoptosis and angiogenesis, elevated expression of alanine aminotransferase (ALT), aspartate aminotransferase (AST) and alkaline phosphatase (ALP), and increased levels of bilirubin (Fig. S1N–U). Notably, no significant differences were found in hepatic lipid accumulation (Fig. S1V, W). Moreover, T cells and macrophages were increased, but not neutrophils (Fig. S2A–I). Thus, 8-week-old *Mcrs1*$^{(\Delta/\Delta)hep}$ mice display fibrotic livers and significant liver injury with loss of hepatocyte proliferative capacity and increased inflammation.

Surprisingly, ~50% of *Mcrs1*$^{(\Delta/\Delta)hep}$ mice died between 8 and 15 weeks of age (Fig. 1B), and they had a cirrhotic phenotype pathologically characterized by the presence of visible regenerative nodules (RNs) (Fig. 1C, D, and supplementary materials and methods)[1]. Further characterization of fibrotic marks confirmed that livers from *Mcrs1*$^{(\Delta/\Delta)hep}$ mice sacrificed at 15±3 weeks of age had strong fibrosis, with *de novo* deposition of ECM surrounding RNs (Fig. 1E–H). *Mcrs1*$^{(\Delta/\Delta)hep}$ mice also exhibited elevated ALT and reduced albumin levels, respectively, indicating that their livers were damaged and dysfunctional (Fig. 1I, J). Moreover, levels of NH_3 were elevated in blood of 8-week-old *Mcrs1*$^{(\Delta/\Delta)hep}$ mice and higher still at 15 weeks of age (Fig. 1K). No signs of necrosis, cholestasis or preneoplastic lesions were observed in 15-week-old *Mcrs1*$^{(\Delta/\Delta)hep}$ mice.

Cirrhosis in 15-week-old *Mcrs1*$^{(\Delta/\Delta)hep}$ mice was additionally characterized by increased angiogenesis and impaired hepatocyte turnover, together with drastic changes in metabolic zonation (Fig. 1E, L and Fig. S3A–C). The arrest of hepatocyte proliferation was accompanied by a pronounced bile duct reaction (Fig. 1E, M). Grading of livers from 15-week-old *Mcrs1*$^{(\Delta/\Delta)hep}$ mice according to an adapted Child-Pugh score indicated that *Mcrs1*$^{(\Delta/\Delta)hep}$ mice had grade 2 and 3 cirrhosis (Fig. S3D–E and supplementary methods). At this time point, the adaptive immune response was resolved, but macrophages and neutrophils were enhanced, likely because of increased cell death (Fig. S3F–I).

Tracing of hepatocytes using the R26_LSL_eYFP reporter line crossed with the *Mcrs1*$^{(\Delta/\Delta)hep}$ mouse confirmed a recombination efficiency of 99,97%±0,03% (Fig. S3J, K). Interestingly, ~50% of RNs were eYFP negative, likely originated from HPCs that differentiated into hepatocytes (Fig. S3L, M)[9], and which retained MCRS1 expression (Fig. S3N). Importantly, no desmin positive fibroblasts co-expressed eYFP, and eYFP positive hepatocytes did present neither loss of E-cadherin nor expressed vimentin (Fig. S3O–R), suggesting that hepatocytes do neither transdifferentiate nor undergo EMT. Thus, the *Mcrs1*$^{(\Delta/\Delta)hep}$ mouse is apparently the first genetic mouse model recapitulating several clinical features of liver cirrhosis.

Expression of BA transporters is deregulated in cirrhotic livers

To determine how MCRS1 loss in hepatocytes promotes cirrhosis, we performed a quantitative proteomic analysis using isobaric tags for relative and absolute quantitation (iTRAQ) in livers from 8-week-old *Mcrs1*$^{(\Delta/\Delta)hep}$ mice (Fig. S4A). Global proteomic profiling identified 4,279 proteins, of which 878 were differentially expressed: 416 and 462 downregulated and upregulated, respectively (Fig. S4B). BA transporters in hepatocytes were heavily represented, with predominant downregulation of NTCP, detected to be the second most differentially downregulated protein in 8-week-old *Mcrs1*$^{(\Delta/\Delta)hep}$ mice (Fig. 2A and Fig. S4B). Expression of *Slc10a1* (NTCP) and *Slco1b2* (OATP1B2), responsible for BA uptake from blood to hepatocytes[5,6], was significantly downregulated in hepatocytes isolated from 8-week-old *Mcrs1*$^{(\Delta/\Delta)hep}$ mice (Fig. 2B–D), whereas expression of *Abcc4* (MRP4), implicated in BA export from hepatocytes to blood, was significantly upregulated (Fig. 2B, C). Notably, *Abcb11* (BSEP), a transporter specialized in BA export from hepatocytes to bile canaliculi, was also downregulated (Fig. 2B, C). Consequently, deregulation of BA flow caused accumulation of total BAs, including the primary BA cholic acid, in blood and liver of *Mcrs1*$^{(\Delta/\Delta)hep}$ mice (Fig. 2E, F), while reducing cholic acid in their intestines and feces (Fig. 2F and Fig. S4C, D). Notably, unchanged blood and liver cholesterol, as well as *Cyp7a1* and *Nr0b2* (SHP) mRNA levels, indicated that BA synthesis, metabolism and signaling in hepatocytes are not altered (Fig. S4E–G)[6]. This was further confirmed by unaffected levels of intestinal *Fgf15* (Fig. S4H)[5,6].

To corroborate these findings, we generated a *Col1a1* knockin mouse expressing human MCRS1 (hMCRS1) via a tetracycline-dependent transactivator controlled by the hepatocyte-specific liver activated protein promoter (Lap) (Fig. S4I). Without doxycycline, hMCRS1 was expressed specifically in hepatocytes (Fig. 2D). These mice were designated "*hMCRS1*$^{(+/KI)hep}$ mice"; littermate controls are referred to "*hMCRS1*$^{(+/+)hep}$ mice". hMCRS1 overexpression in hepatocytes substantially increased NTCP levels, and mirrored the changes observed in the expression pattern of BA transporter genes in 8-week-old *Mcrs1*$^{(\Delta/\Delta)hep}$ mice (Fig. 2D, G, H and Fig. S4G). MCRS1 depletion in hepatocytes thus induces BA accumulation in blood by specifically changing the expression pattern of BA transporters, independently of BA synthesis.

Importantly, NTCP was downregulated 1 week after MCRS1 depletion in isolated hepatocytes of asymptomatic 6-week-old *Mcrs1*$^{(\Delta/\Delta)hep}$ mice (Fig. S5A–D). While no differences in ALT and BA levels were detected at this time, they increased steadily 2 and 3 weeks after MCRS1 depletion (Fig. S5E, F). However, neither ductular reaction nor inflammation was detected in 1-week-old *Mcrs1*$^{(\Delta/\Delta)hep}$ mice (Fig. S5G–K). Therefore, dysregulation of the BA transporters is an early event triggering increased BA levels, prior to proliferation arrest of hepatocytes, inflammation and expansion of HPCs.

To demonstrate the importance of perturbing BA flow in cirrhosis, NTCP was re-expressed in 8-week-old *Mcrs1*$^{(\Delta/\Delta)hep}$ mice via hydrodynamic tail vein injection (Fig. 2I, J). NTCP overexpression normalized BA levels, prevented fibrosis, and cirrhosis was not detected in 15-week-old *Mcrs1*$^{(\Delta/\Delta)hep}$ mice (Fig. 2K–O). Moreover, ~90% of *Mcrs1*$^{(\Delta/\Delta)hep}$ mice overexpressing NTCP survived over 15 weeks of age, while more than 50% of *Mcrs1*$^{(\Delta/\Delta)hep}$ mice died before (Fig. 2P). Thus, restoring BA homeostasis by re-expressing NTCP in

Mcrs1$^{(\Delta/\Delta)hep}$ mice was sufficient to reduce fibrosis and extend mouse survival. NTCP downregulation and perturbation of BA flow are hence the causal links between MCRS1 loss and cirrhosis development.

Secondary BAs might not influence the *Mcrs1*$^{(\Delta/\Delta)hep}$ mouse phenotype

To exclude the possibility that secondary BAs influence the development of cirrhosis, *Mcrs1*$^{(\Delta/\Delta)hep}$ mice were fed a diet containing cholestyramine resin (ChR) (Fig. S6A), a well-known BA sequestrant used in patients with liver diseases[5]. While ChR-fed *Mcrs1*$^{(\Delta/\Delta)hep}$ mice exhibited early body weight loss, their body weight recovered over time (Fig. S6B). Strikingly, although ChR impaired BA recycling and initially reduced blood BA levels in *Mcrs1*$^{(\Delta/\Delta)hep}$ mice, BAs accumulated over time in the blood of ChR-fed *Mcrs1*$^{(\Delta/\Delta)hep}$ mice to the same extent as in normal diet (ND)-fed *Mcrs1*$^{(\Delta/\Delta)hep}$ mice (Fig. S6C, D). Moreover, ChR-fed *Mcrs1*$^{(\Delta/\Delta)hep}$ mice had apparently cirrhotic livers with high levels of ALT, and a considerably higher frequency of cirrhosis than their ND-fed counterparts (Fig. S6E–G). However, the adapted Child-Pugh score indicated similar grades of cirrhosis in both ChR- and ND-fed *Mcrs1*$^{(\Delta/\Delta)hep}$ mice (Fig. S6H), suggesting that ChR treatment does not aggravate cirrhosis severity. ChR-fed *Mcrs1*$^{(\Delta/\Delta)hep}$ mice also exhibited lower survival than ND-fed *Mcrs1*$^{(\Delta/\Delta)hep}$ mice (Fig. S6I). Notably, the secondary BA, deoxycholic acid (DCA), was significantly reduced over time in feces of ChR-fed *Mcrs1*$^{(\Delta/\Delta)hep}$ mice at 15 and 22 weeks of age when compared to ND-fed mice (Fig. S6J). This indicates an efficient BA chelation in the intestine, and suggests that secondary BAs are unlikely playing a major role in cirrhosis development. Moreover, despite BAs can be chelated and their levels are significantly reduced, the inhibition of BA uptake observed in hepatocytes of *Mcrs1*$^{(\Delta/\Delta)hep}$ mice seems to be sufficient to increase blood BAs overtime, triggering fibrosis in the liver. Therefore, ChR cannot prevent blood BA accumulation in *Mcrs1*$^{(\Delta/\Delta)hep}$ mice and hence, intestinal chelation of BAs might not be an effective treatment against cirrhosis.

Increased blood BAs exacerbate the *Mcrs1*$^{(\Delta/\Delta)hep}$ mouse phenotype

Since reducing BA levels in blood by re-expressing NTCP in *Mcrs1*$^{(\Delta/\Delta)hep}$ mice rescues cirrhosis, we next reasoned that increasing their concentration in the liver would exacerbate the cirrhotic phenotype of *Mcrs1*$^{(\Delta/\Delta)hep}$ mice. We therefore triggered bile duct injury and bile leakage in livers by genetically suppressing the MDR2 transporter in *Mcrs1*$^{(\Delta/\Delta)hep}$ mice, crossing *Abcb4* (MDR2) knockout mice (*Abcb4*$^{(-/-)}$) with *Mcrs1*$^{(\Delta/\Delta)hep}$ mice, generating homozygous *Mcrs1*$^{(\Delta/\Delta)hep}$;*Abcb4*$^{(-/-)}$ mice (Fig. S7A). MDR2 is a transporter of phosphatidylcholine, which forms micelles around hydrophobic BAs and represent a protective shield to the cells composing the liver bile canaliculi and gallbladder. Loss of MDR2 results into free acidic bile salts in liver bile canaliculi, which disrupt the membranes of bile duct cells, triggering bile leakage. While *Abcb4*$^{(-/-)}$ mice develop hepatic lesions resembling primary sclerosing cholangitis and spontaneously progress to severe biliary fibrosis, the phenotypic perturbations of *Mcrs1*$^{(\Delta/\Delta)hep}$;*Abcb4*$^{(-/-)}$ mice were profoundly accelerated, with jaundice reflected by yellowish peritoneum and earlier death (Fig. S7B, C). Moreover, higher total blood BAs, and plasma and liver cholic acid levels were detected

(Fig. S7D–F). Direct and total bilirubin were also increased (Fig. S7G, H). This was accompanied by severe fibrosis and a stronger bile duct reaction (Fig. S7I–L).

To confirm these findings, *Mcrs1*$^{(\Delta/\Delta)hep}$ mice were fed with a BA-supplemented diet (BD) for 4 weeks after tamoxifen treatment (Fig. S8A). BA supplementation increased plasma and liver cholic acid, ALT, and bilirubin in *Mcrs1*$^{(+/+)hep}$ mice, which were further enhanced in *Mcrs1*$^{(\Delta/\Delta)hep}$ mice (Fig. S8B–G). Expectedly, BA supplementation induced fibrosis in *Mcrs1*$^{(+/+)hep}$ mice, that was worsened in BA-fed *Mcrs1*$^{(\Delta/\Delta)hep}$ mice (Fig. S8H–J). Therefore, high levels of BAs trigger liver fibrosis, and exacerbate the phenotypic consequences of knocking out MCRS1 in mouse livers.

FXR predominantly labels human and mouse HSCs

BAs bind to and activate FXR[5,6]. Single-nuclei RNA sequencing (snRNA-seq) performed in human livers surprisingly revealed that *NR1H4* (FXR) was predominantly expressed in HSCs (Fig. 3A–D, Fig. S9A and Table S2). Notably, expression of other well-known BA receptors was not detected (Fig. S9B–D)[5,6]. Likewise, single cell (sc) RNA-seq conducted in liver tissue from healthy mouse confirmed that only *Nr1h4* was mainly expressed in HSCs (Fig. 3E–H and Fig. S9E–G). Further analysis from publicly available scRNA-seq data sets[10] confirmed the expression of *Nr1h4* in liver fibroblasts (Fig. 3I, J). Finally, co-IHC using FXR and desmin in *Mcrs1*$^{(\Delta/\Delta)hep}$ mice revealed the presence of FXR in 50% of HSCs (Fig. S9H, I). Interestingly, *SLC10A1* (NTCP) was detected neither in human nor in mouse HSCs (Fig. S9J, K), confirming previous data[11,12], and indicating that other transporters are implicated in BA transport into HSCs. Therefore, activation of FXR in HSCs by BAs could have an unexpected pathophysiological role in liver fibrosis.

BAs activate FXR in HSCs to promote liver fibrosis

We therefore genetically targeted *Nr1h4* in HSCs by crossing the *Nr1h4* conditional knockout mouse (*Nr1h4* lox) with a transgenic mouse in which cre expression was driven by the lecithin-retinol acyltransferase (Lrat) promoter, reportedly expressed in HSCs (Lrat-cre mouse), and as revealed by scRNA-seq (Fig. 3E), giving *Nr1h4*$^{(\Delta/\Delta)HSC}$ mice (Fig. 4A). Specific ablation of *Nr1h4* in HSCs was corroborated in isolated HSCs and liver sections (Fig. 4B–E). Notably, loss of FXR was detected neither in hepatocytes nor in immune cells, that apparently did not express FXR, as also confirmed by scRNA-seq (Fig. 3B–D, F-H and Fig. S10A–C). Since crossing *Nr1h4*$^{(\Delta/\Delta)HSC}$ and *Mcrs1*$^{(\Delta/\Delta)hep}$ mice would lead to deletion of MCRS1 and FXR in both hepatocytes and HSCs, *Nr1h4*$^{(\Delta/\Delta)HSC}$ mice were subjected to BDL (Fig. 4F). The liver phenotype of *Nr1h4*$^{(\Delta/\Delta)HSC}$ mice with BDL was similar to that of *Nr1h4*$^{(+/+)HSC}$ mice with BDL, and there were no differences in their: liver to body weight ratios; survival; levels of ALT, blood BAs, total bilirubin; or bile duct reaction, which was elevated in both cases (Fig. S10D–K). This suggests that abolishing FXR signaling in HSCs does not impair liver injury. However, fibrosis was strongly suppressed in *Nr1h4*$^{(\Delta/\Delta)HSC}$ mice with BDL (Fig. 4G, H). Interestingly, further analysis showed that bile duct-ligated *Nr1h4*$^{(+/+)HSC}$ mice had a decrease of NTCP (*Slc10a1*) expression in isolated hepatocytes (Fig. 4I, J). This confirms that BDL leads to BA accumulation, which feedbacks to hepatocytes, acts on FXR, and suppresses NTCP expression, a well-known target gene

negatively regulated by FXR in hepatocytes[5]. Therefore, BAs activate FXR signaling in HSCs, stimulating HSC transdifferentiation into myofibroblasts to provoke liver fibrosis.

To corroborate these findings, FXR was overexpressed in the HSC line LX-2. Overexpression of FXR significantly induced fibrotic marks in LX-2 cells (Fig. S11A, B). Next, MCRS1 was downregulated in the hepatocyte cell line HepG2, and medium conditioned with these cells was used to culture LX-2 cells, in which FXR was depleted via the use of siRNA (Fig. 4K and Fig. S11C, D). MCRS1-depleted HepG2 cells had lower NTCP levels than HepG2 cells treated with control siRNA, and their conditioned medium contained higher levels of primary BAs than control conditioned medium (Fig. 4L and Fig. S11E). Interestingly, FXR-depleted LX-2 cells cultured in BA-enriched conditioned medium from MCRS1-depleted HepG2 cells exhibited lower *ACTA2*, *COL1A1* and *COL3A1* expression than siRNA control-treated cells (Fig. 4M, N and Fig. S11F, G). Re-expression of NTCP in MCRS1-depleted HepG2 cells reduced BA levels in their conditioned medium (Fig. 4L and Fig. S11H). When LX-2 cells were grown in conditioned medium from MCRS1-depleted HepG2 cells with overexpression of NTCP, their *ACTA2*, *COL1A1* and *COL3A1* expression was significantly reduced in an FXR-dependent manner (Fig. 4M, N and Fig. S11G, H). Interestingly, chelating BAs using ChR in the HepG2 culture medium abolished the expression of fibrotic marks, independently of MCRS1, NTCP or FXR expression (Fig. 4M, N and Fig. S11G, H).

Same data were obtained when isolated HSCs from $Nr1h4^{HSC}$ mice were cultured with conditioned medium of isolated hepatocytes from $Mcrs1^{hep}$ mice (Fig. 4O–Q and Fig. S11I–K). Conditioned medium from isolated hepatocytes from $Mcrs1^{(\Delta/\Delta)hep}$ mice overexpressing NTCP (Fig. 2I) abrogated fibrotic marks in HSCs from $Nr1h4^{HSC}$ mice (Fig. 4O–Q and Fig. S11K). Taken together, these data indicate that MCRS1 loss in hepatocytes downregulates NTCP, leading to BA efflux, which in turn stimulates HSCs via FXR activation.

MCRS1 overexpression ameliorates liver fibrosis

Since $hMCRS1^{(+/KI)hep}$ mice showed an increase of NTCP levels (Fig. 2D), and mirrored the changes observed in $Mcrs1^{(\Delta/\Delta)hep}$ mice, we hypothesized that $hMCRS1^{(+/KI)hep}$ mice might be protected against liver fibrosis. Hence, 10-week-old $hMCRS1^{(+/+)hep}$ and $hMCRS1^{(+/KI)hep}$ mice were subjected to BDL (Fig. S12A). Whereas BDL downregulated NTCP in isolated hepatocytes, bile duct-ligated $hMCRS1^{(+/KI)hep}$ mice partially recovered NTCP expression (Fig. 4I, J and Fig. S12B). Notably, BDL did not further increase cholestasis (determined by gallbladder size and number of $CK7^+$ cells and biliary ducts in the lumen) in $hMCRS1^{(+/KI)hep}$ mice when compared to littermate controls (Fig. S12C–F). However, bile duct-ligated $hMCRS1^{(+/KI)hep}$ mice had significantly lower levels of primary BAs in blood, and liver injury and fibrosis were ameliorated when compared to bile duct-ligated $hMCRS1^{(+/+)hep}$ mice (Fig. S12C–N). The same outcome was observed in mice obtained by crossing $hMCRS1^{hep}$ and $Abcb4^{(-/-)}$ mice (Fig. S12O–S). These results indicate that MCRS1 regulates NTCP-mediated BA flow, critical in fibrosis pathogenesis.

MCRS1 regulates histone acetylation of BA transporter genes

Protein sequence analysis revealed a previously unrecognized SANT (standing for switching-defective protein 3 (Swi3), adaptor 2 (Ada2), nuclear receptor co-repressor (N-CoR), transcription factor (TFIIIB)) domain in MCRS1. The SANT domain is found in chromatin remodeling proteins that interact with histones and closely resembles the DNA-binding domain (DBD) of Myb-related proteins (Fig. 5A, B and Fig. S13A). The SANT domain thus has a central role in chromatin remodeling, functioning as a unique histone-interaction module that couples histone binding to deacetyltransferase activity[13]. To check this, we transfected the HepG2 and Huh7 hepatocyte cell lines with full-length HA-tagged-MCRS1 (HA-MCRS1^{WT}) and mutant HA-tagged-MCRS1 lacking the SANT domain (HA-MCRS1$^{\Delta 130–192}$). Protein expression of HA-MCRS1^{WT} and HA-MCRS1$^{\Delta 130–192}$ constructs was similar and localized to the nucleus (Fig. S13B, C). Immunoprecipitation assays using HA antibody and blotting with a specific MCRS1 antibody revealed that the SANT domain was required for the interaction between MCRS1 and Histone H3 (HISH3) (Fig. 5C and Fig. S13D). Next, direct HISH3 binding to MCRS1 was tested. Recombinant glutathione S-transferase (GST), GST-tagged-MCRS1^{WT} or GST-tagged-MCRS1$^{\Delta 130–192}$ were incubated with *in vitro* translated (IVT) HA-tagged-HISH3. Pulldown assay revealed that GST-MCRS1^{WT} interacted with HISH3, but this interaction was considerably reduced with GST-MCRS1$^{\Delta 130–192}$ (Fig. 5D), indicating that HISH3 binds directly to MCRS1 via SANT domain.

Interestingly, HDAC1 immunoprecipitated with HA-MCRS1^{WT} but not with HA-MCRS1$^{\Delta 130–192}$ (Fig. 5C), indicating that MCRS1, HDAC1 and HISH3 form a trimeric complex, in which MCRS1 connects HDAC1 to HISH3 via the SANT domain. Additionally, whereas Pontin and Reptin co-immunoprecipitated with both HA-MCRS1^{WT} and HA-MCRS1$^{\Delta 130–192}$, members of neither the NSL complex (MOF, KANSL1 and KANSL3) nor INO80 were detected in the immunoprecipitates of overexpressing HA-tagged MCRS1 constructs (Fig. 5C). However, MOF, KANSL3, Pontin, Reptin, and HISH3 interacted with endogenous MCRS1 (Fig. 5E). Taken together, these data indicate that MCRS1 might act as a histone acetylation regulator by anchoring HDAC1 to HISH3, apparently in an INO80/NSL-independent manner.

In accordance with these findings, histone acetylation (normalized to total HISH3) was substantially increased in core histone extracts from HepG2 cells overexpressing HA-MCRS1$^{\Delta 130–192}$ but not in cells overexpressing HA-MCRS1^{WT} (Fig. 5F). Additionally, hepatocytes isolated from *Mcrs1*$^{(\Delta/\Delta)hep}$ mice 1 week after MCRS1 deletion, showed significantly increased histone acetylation, without downregulating HDAC1 expression (Fig. 5G). Moreover, an *in vitro* histone acetylation assay conducted in the presence of HA-MCRS1^{WT} or HA-MCRS1$^{\Delta 130–192}$ showed that MCRS1 lacks intrinsic histone deacetylase activity (Fig. S13E). Thus, increased histone acetylation after MCRS1 loss is a very early event, and MCRS1 anchors HDAC1 and HISH3 via the SANT domain. SANT domain deletion, like MCRS1 depletion, seemingly releases HDAC1 from HISH3, increasing histone acetylation.

To determine whether increased histone lysine acetylation affects the expression of BA transporter genes, we performed several chromatin immunoprecipitation (ChIP) assays in

HepG2 and Huh7 cells. Interestingly, MCRS1 was enriched in regulatory regions of BA transporter genes (Fig. 5H and Fig. S13F). ChIP experiments using anti-acetylated H3K9 and H3K18 antibodies in HepG2 cells overexpressing either HA-MCRS1^{WT} or the HA-MCRS1$^{\Delta 130–192}$ mutant showed that cells overexpressing HA-MCRS1$^{\Delta 130–192}$ exhibited increased histone lysine acetylation in regulatory regions of BA transporter genes (Fig. 5I, J). To relate the increase of histone acetylation to the loss of interaction of HDAC1 with the BA transporter genes, we performed ChIP experiments using HDAC1 antibody in HepG2 cells treated with siRNA against *MCRS1* (Fig. 5K and Fig. S13G). MCRS1 knockdown reduced HDAC1 binding to BA transporter genes (Fig. 5K). Thus, MCRS1 might be essential for synchronizing lysine histone deacetylation with transcription of BA transporters via its direct binding to HISH3.

Next, we checked whether downregulation of *SLC10A1* expression was associated with increased chromatin repressive marks. No differences were detected in H3K9me2, H3K9me3 and H3K27me3 in *MCRS1*- and control-siRNA-treated cells (Fig. S13G–J). Therefore, downregulation of NTCP upon MCRS1 depletion is likely mediated by gene histone acetylation independently of chromatin repressive marks.

MCRS1 and NTCP expressions correlate in human cirrhosis

To clarify the clinical relevance of our findings, we analyzed MCRS1 expression and NTCP status in two different gene datasets from various liver cirrhotic patients (GSE77627 -14 healthy and 22 cirrhotic samples-, and GSE20140 -307 cirrhotic samples). Analysis of GSE77627 dataset indicated that *SLC10A1* expression was significantly downregulated in human cirrhosis when compared to healthy controls (Fig. S14A). Moreover, *MCRS1* expression correlated with *SLC10A1* and *ACTA2* in both datasets (Fig. S14B–E). Although loss of MCRS1 expression was never detected in cirrhotic samples, further analysis of 10 healthy and 50 cirrhotic human livers (Table S3) showed that MCRS1 was mainly nuclear in healthy livers but was diffused throughout the cytoplasm in cirrhotic livers (Fig. S14F–H). Additionally, cytoplasmic MCRS1 correlated significantly with fibrosis marks in these samples (Fig. S14I, J). Therefore, loss of nuclear MCRS1 as well as decreased NTCP levels in human livers might be critical for cirrhosis, and dysregulation of BA flow might represent a central, conserved and universal signaling event in human cirrhotic development.

Discussion

To our knowledge, the *Mcrs1*$^{(\Delta/\Delta)hep}$ mouse is the first genetic model of liver cirrhosis. Using this model, we show that histone acetylation-mediated NTCP downregulation in hepatocytes is a primary event triggering liver fibrosis, preceding liver injury and inflammation. Downregulation of NTCP leads to aberrant distribution of the BA pool, and sinusoidal BA accumulation activates FXR in HSCs to promote liver fibrosis.

Human data demonstrates that this mechanism is universally relevant to the variety of ways cirrhosis is induced, and will impact the clinical research to open new avenues for the development of anti-fibrotic treatments and prevention of cirrhosis. Interestingly, obeticholic acid (OA), a semi-synthetic primary BA analogue and potent FXR ligand, was recently approved by the American Food and Drug Administration (FDA) under the name Ocaliva^{R},

and is in phase 2/3 clinical studies for cirrhosis[14,15]. OA supposedly exert beneficial effects by activating FXR in hepatocytes and intestinal epithelial cells[16]. However, recent clinical data alerted the FDA on adverse effects of OA: its use caused severe fibrosis and fulminant liver damage in some patients. Although more research is needed to understand the effects of primary BAs in other liver cell types to ensure that patients can be safely and effectively treated with Ocaliva^{R}, our data indicate that BAs are important in HSC activation and fibrosis, and represent a real paradigm shift with high impact on future therapeutic strategies.

MCRS1 loss or deletion of its SANT domain leads to release of HDAC1 from its anchoring sites on HISH3, preventing histone deacetylation of BA transporter genes. Our data suggest that MCRS1 binds to specific regulatory regions of genes and orchestrates their transcriptional activity, likely in coordination with chromatin remodelers and transcription factors. Transcriptionally active genes are tightly regulated by post-translational chromatin modifications, and in particular by reversible lysine acetylation of histones, which increases accessibility to the transcription machinery. However, enhanced lysine acetylation does not always correlate with increased target gene transcription. Previous work has shown that transcriptional activation is not necessarily associated with increased acetylation[17]. Indeed, some genes could be downregulated by histone acetylation[18] such as individual activators could confer distinct patterns of histone acetylation on target promoters[19]. Enhanced lysine acetylation of HISH3 and HISH4 lysine residues upon MCRS1 depletion or SANT domain deletion could be implicated in either gene activation or gene repression. Actually, histone acetylation decreases expression of *Scl10a1*, but increases expression of *Abcc4* in *Mcrs1*$^{(\Delta/\Delta)hep}$ mice (Fig. 2C). It is hence tempting to speculate that histone acetylation, likely with the cooperation of enhancers and other regulators, might be implicated in the control of gene expression. Despite genome-wide ChIP-sequencing experiments have been conducted in mouse embryonic stem cells[20], identifying potential MCRS1 target genes in hepatocytes would give more insights into the role of MCRS1 in gene regulation.

It should also be noted that SANT domain deletion appears to be functionally equivalent to MCRS1 depletion. In agreement with this, a shift of MCRS1 from nucleus to cytoplasm was found in human cirrhosis. This goes in line with recent work indicating that MCRS1 may be localized in different sub-cellular compartments[8]. Interestingly, MCRS1 regulates mTORC1 activity at the lysosomal surface in response to amino acids[21], leading us to speculate that nutritional cues could direct MCRS1 to promoters of specific genes, regulating their transcriptional activity. In this context, it is notable that branched-chain amino acid-based medicine has shown positive results in patients with cirrhosis[22].

In sum, MCRS1 is a histone acetylation regulator that anchors HDAC1 to HISH3 via a previously undescribed SANT domain, playing a key role in proper modulation of gene expression and liver health. Loss of MCRS1 in hepatocytes induces liver cirrhosis by increasing histone lysine acetylation of BA transporter genes, accumulating BAs in liver sinusoids to activate FXR on HSCs. Human patient data demonstrate that this mechanism could be general for liver cirrhosis in humans, and targeting histone acetylation in liver cirrhotic patients by inhibiting histone acetyl transferases could be a viable remedial option for this deadly disease.

Supplementary Material

Refer to Web version on PubMed Central for supplementary material.

Acknowledgments

We thank all mouse providers. We acknowledge the patients and the BioBank Hospital Ramón y Cajal-IRYCIS (B.0000678), as well the CNIO Biobank, integrated in the Spanish National Biobanks Network and Biomodels Platform of the ISCIII. We are also thankful to the CNIO Mouse Genome Editing Core Unit and Animal Facility for the mouse re-derivation and maintenance, respectively.

Financial support

A.G. is a recipient of Severo Ochoa PhD fellowship. E.K is a recipient of fellowships from the National Research Foundation (NRF) from the Korean Ministry of Education (2020R1A6A3A03037725) and the CNIO-friends, supported by Severo Ochoa32 CNIO funds. This work was funded by grants to N.D. from the European Foundation for the Study of Diabetes (EFSD) award supported by EFSD/JRDF/Lilly programme (EASD 96103), from the Comunidad Autónoma de Madrid (S2017/BMD-3817) and, from the State Research Agency (AEI, 10.13039/501100011033) from the Spanish Ministry of Science and Innovation (projects SAF2016-76598-R, SAF2017-92733-EXP, RTI2018-094834-B-I00 and RED2018-102723-T), cofunded by European Regional Development Fund (ERDF) and from the Asociación Española Contra el Cáncer (AECC) (project PRYGN211184DJOU). This work was developed at the CNIO funded by the Health Institute Carlos III (ISCIII) and the Spanish Ministry of Science and Innovation. G.P.V. was supported by a grant from the State Research Agency from the Spanish Ministry of Science and Innovation (projects PID2019-105173RB42 I00). B.I. was supported by the National Institute of Health, National Cancer Institute (R37CA258829, R21CA263381). R.F.S was funded by NIH grants (1R01DK128955, 5R01DK124104 and 1R01CA262424).

Data availability

All data are available in the main text or Methods. Materials are available upon request to N.D. and sharing materials will be subject to standard material transfer agreements. Mass spectrometry proteomics data have been deposited to the ProteomeXchange Consortium via the PRIDE [1] partner repository with the dataset identifier PXD023026 (**Username**: reviewer_pxd023026@ebi.ac.uk; **Password**: BqiMEJnA). snRNA- and scRNA-seq data have been deposited to the NCBI with the GEO accession number GSE179548 (**Link**: https://www.ncbi.nlm.nih.gov/geo/query/acc.cgi?acc=GSE179548; **Token**: evaliwkctjkbfcl) and GSE158183 GSM4794841, respectively.

Abbreviations

ALP	Alkaline phosphatase
ALT	Alanine aminotransferase
AST	Aspartate aminotransferase
BA	Bile acid
BSEP	Bile salt export pump
ChIP	Chromatin immunoprecipitation
DCA	Deoxycholic acid
ECM	Extracellular matrix

FDA	Food and Drug Administration
FXR	Farnesoid X receptor
GST	Glutathione S-transferase
HA-MCRS1$^{\Delta 130–192}$	HA-tagged-MCRS1 lacking the SANT domain
HA-MCRS1^{WT}	full-length HA-tagged-MCRS1
HDAC1	Histone deacetylase 1
HISH3	histone H3
HPCs	Hepatic progenitor cells
HSCs	Hepatic stellate cells
iTRAQ	isobaric tags for relative and absolute quantitation
IVT	*in vitro* translated
KANSL1 and KANSL3	KAT8 regulatory NSL complex subunits 1 and 3
MCRS1	Microspherule 1
MOF	males absent on the first
MRP2/3	Multidrug resistance-associated protein 2/3
MRP3, MRP4	Multidrug resistance-associated proteins 3 and 4
NSL	Non-specific lethal
NTCP	Na^+-taurocholate cotransporting polypeptide
OA	Obeticholic acid
OATP	Organic anion transporting polypeptides
OST	Organic solute transporter
RNs	Regenerative nodules
SANT	Switching-defective protein 3 (Swi3), adaptor 2 (Ada2), nuclear receptor co-repressor (N-CoR), transcription factor (TFIIIB)
SC	Single cell
snRNA-seq	Single-nuclei RNA sequencing
TSSs	Transcription start sites
WB	Western blot
WDR5	WD repeat-containing protein 5

References

[1]. Garrido A, Djouder N. Cirrhosis: A Questioned Risk Factor for Hepatocellular Carcinoma. Trends Cancer 2021;7:29–36. [PubMed: 32917550]

[2]. Giallourakis CC. Liver complications in patients with congestive heart failure. Gastroenterol Hepatol 2013;9:244–246.

[3]. Karlsen TH, Lammert F, Thompson RJ. Genetics of liver disease: From pathophysiology to clinical practice. J Hepatol 2015;62:S6–S14. [PubMed: 25920091]

[4]. Liberal R, Grant CR. Cirrhosis and autoimmune liver disease: Current understanding. World J Hepatol 2016;8:1157–1168. [PubMed: 27729952]

[5]. de Aguiar Vallim TQ, Tarling EJ, Edwards PA. Pleiotropic roles of bile acids in metabolism. Cell Metab 2013;17:657–669. [PubMed: 23602448]

[6]. Shapiro H, Kolodziejczyk AA, Halstuch D, Elinav E. Bile acids in glucose metabolism in health and disease. J Exp Med 2018;215:383–396. [PubMed: 29339445]

[7]. Shi Y, Sun H, Bao J, Zhou P, Zhang J, Li L, et al. Activation of inactive hepatocytes through histone acetylation: a mechanism for functional compensation after massive loss of hepatocytes. Am J Pathol 2011;179:1138–1147. [PubMed: 21763259]

[8]. Sheikh BN, Guhathakurta S, Akhtar A. The non-specific lethal (NSL) complex at the crossroads of transcriptional control and cellular homeostasis. EMBO Rep 2019;20:e47630. [PubMed: 31267707]

[9]. Tummala KS, Brandt M, Teijeiro A, Graña O, Schwabe RF, Perna C, et al. Hepatocellular Carcinomas Originate Predominantly from Hepatocytes and Benign Lesions from Hepatic Progenitor Cells. Cell Reports 2017;19:584–600. [PubMed: 28423321]

[10]. Buechler MB, Pradhan RN, Krishnamurty AT, Cox C, Calviello AK, Wang AW, et al. Cross-tissue organization of the fibroblast lineage. Nature 2021;593:575–579. [PubMed: 33981032]

[11]. Kordes C, Sawitza I, Gotze S, Herebian D, Haussinger D. Hepatic stellate cells contribute to progenitor cells and liver regeneration. J Clin Invest 2014;124:5503–5515. [PubMed: 25401473]

[12]. Fickert P, Fuchsbichler A, Moustafa T, Wagner M, Zollner G, Halilbasic E, et al. Farnesoid X receptor critically determines the fibrotic response in mice but is expressed to a low extent in human hepatic stellate cells and periductal myofibroblasts. Am J Pathol 2009;175:2392–2405. [PubMed: 19910507]

[13]. Boyer LA, Langer MR, Crowley KA, Tan S, Denu JM, Peterson CL. Essential role for the SANT domain in the functioning of multiple chromatin remodeling enzymes. Mol Cell 2002;10:935–942. [PubMed: 12419236]

[14]. Hirschfield GM, Mason A, Luketic V, Lindor K, Gordon SC, Mayo M, et al. Efficacy of obeticholic acid in patients with primary biliary cirrhosis and inadequate response to ursodeoxycholic acid. Gastroenterology 2015;148:751–761. [PubMed: 25500425]

[15]. Kowdley KV, Luketic V, Chapman R, Hirschfield GM, Poupon R, Schramm C, et al. A randomized trial of obeticholic acid monotherapy in patients with primary biliary cholangitis. Hepatology 2018;67:1890–1902. [PubMed: 29023915]

[16]. Khanna A, Jones DE. Novel strategies and therapeutic options for the management of primary biliary cholangitis. Therap Adv Gastroenterol 2017;10:791–803.

[17]. Deckert J, Struhl K. Histone acetylation at promoters is differentially affected by specific activators and repressors. Mol Cell Biol 2001;21:2726–2735. [PubMed: 11283252]

[18]. Reamon-Buettner SM, Borlak J. A new paradigm in toxicology and teratology: altering gene activity in the absence of DNA sequence variation. Reprod Toxicol 2007;24:20–30. [PubMed: 17596910]

[19]. Kaimori JY, Maehara K, Hayashi-Takanaka Y, Harada A, Fukuda M, Yamamoto S, et al. Histone H4 lysine 20 acetylation is associated with gene repression in human cells. Sci Rep 2016;6:24318. [PubMed: 27064113]

[20]. Chelmicki T, Dundar F, Turley MJ, Khanam T, Aktas T, Ramirez F, et al. MOF-associated complexes ensure stem cell identity and Xist repression. Elife 2014;3:e02024. [PubMed: 24842875]

[21]. Fawal MA, Brandt M, Djouder N. MCRS1 binds and couples rheb to amino acid-dependent mTORC1 activation. Dev Cell 2015;33:67–82. [PubMed: 25816988]

[22]. Tajiri K, Shimizu Y. Branched-chain amino acids in liver diseases. Transl Gastroenterol Hepatol 2018;3:47. [PubMed: 30148232]

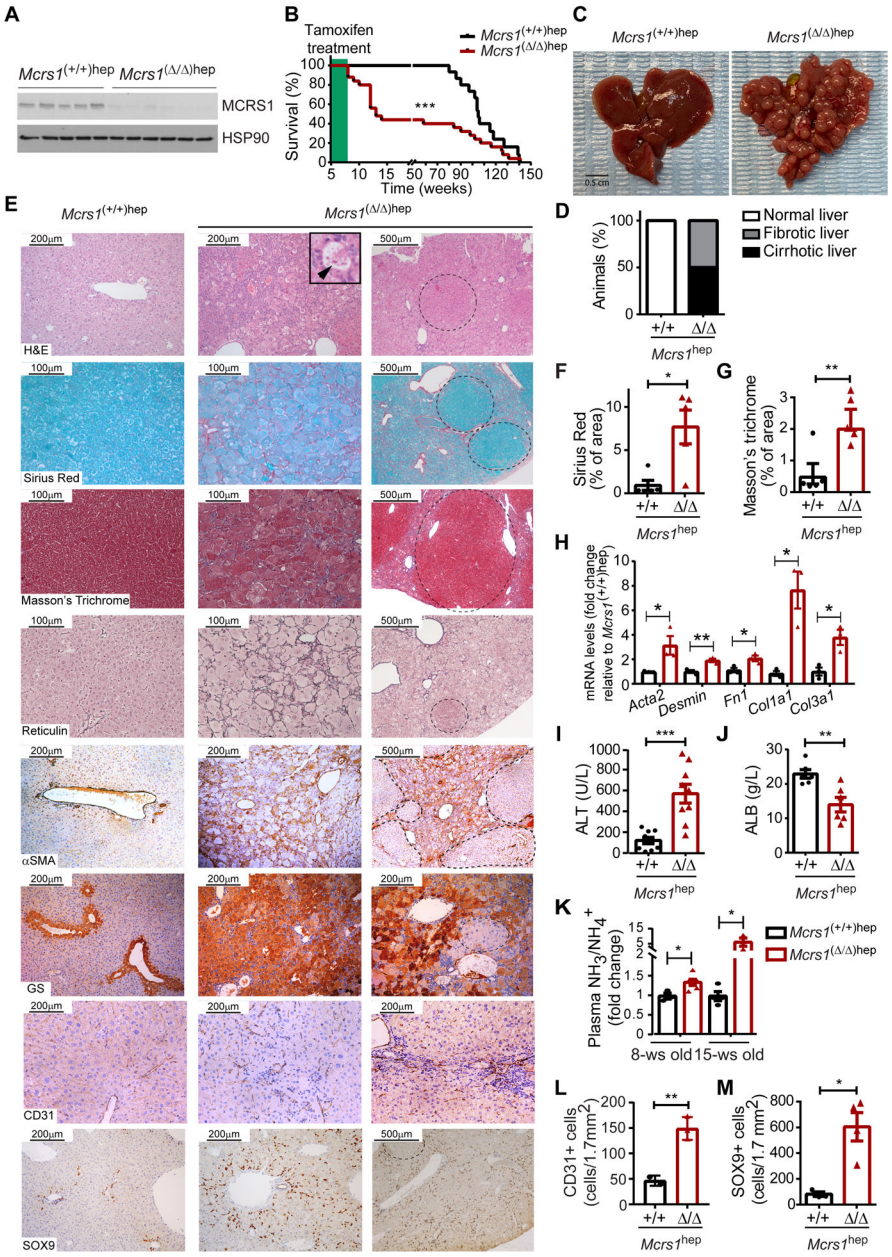

Fig. 1. MCRS1 loss in hepatocytes promotes cirrhosis.

(A) WB from 8-week-old *Mcrs1*$^{(+/+)hep}$ and *Mcrs1*$^{(\Delta/\Delta)hep}$ mouse livers. (B) Survival of *Mcrs1*$^{(+/+)hep}$ and *Mcrs1*$^{(\Delta/\Delta)hep}$ mice (n=15,25). (C) Representative pictures of livers from 15-week-old *Mcrs1*$^{(+/+)hep}$ and *Mcrs1*$^{(\Delta/\Delta)hep}$ mice. (D) Percentage of *Mcrs1*$^{(+/+)hep}$ and *Mcrs1*$^{(\Delta/\Delta)hep}$ mice with cirrhosis at 15 weeks of age (n=15,9). (E) Representative pictures of indicated stainings and IHC of livers from 15-week-old *Mcrs1*$^{(+/+)hep}$ and *Mcrs1*$^{(\Delta/\Delta)hep}$ mice. Arrowhead points a Mallory-Denk body. Dashed lines delimit regenerative nodules. (F) and (G) Quantification of Sirius Red (F) and Masson's Trichrome (F) stainings described in (E) (n=5). (H) Relative mRNA levels of fibrotic markers of hepatocytes isolated from 15-week-old *Mcrs1*$^{(+/+)hep}$ and *Mcrs1*$^{(\Delta/\Delta)hep}$ mice (n=3). (I) and (J) Blood alanine aminotransferase (ALT) (n=9) and albumin (ALB) (n=6) levels from 15-week-old

Mcrs1$^{(+/+)hep}$ and *Mcrs1*$^{(\Delta/\Delta)hep}$ mice. (K) Plasma ammonia (NH_3/NH_4^+) levels from 8- and 15-week-old *Mcrs1*$^{(+/+)hep}$ and *Mcrs1*$^{(\Delta/\Delta)hep}$ mice (n=3,6,4,3). (L) and (M) Quantification of CD31 (L) (n=3) and SOX9 (M) (n=3,4) IHC described in (E). Scale bar: 0.5 cm in (C), 200 and 500 μm in H&E, αSMA and SOX9 pictures, 200 μm in GS and CD31 pictures, and 100 and 500 μm in Sirius Red, Masson's Trichrome and Reticulin pictures. Statistical analysis was performed using Mantel-Cox test in (B), and unpaired two-tailed Student's t test in (F) to (M). Data are represented as means±SEM. *, p≤0.05; **, p≤0.01; ***, p≤0.001.

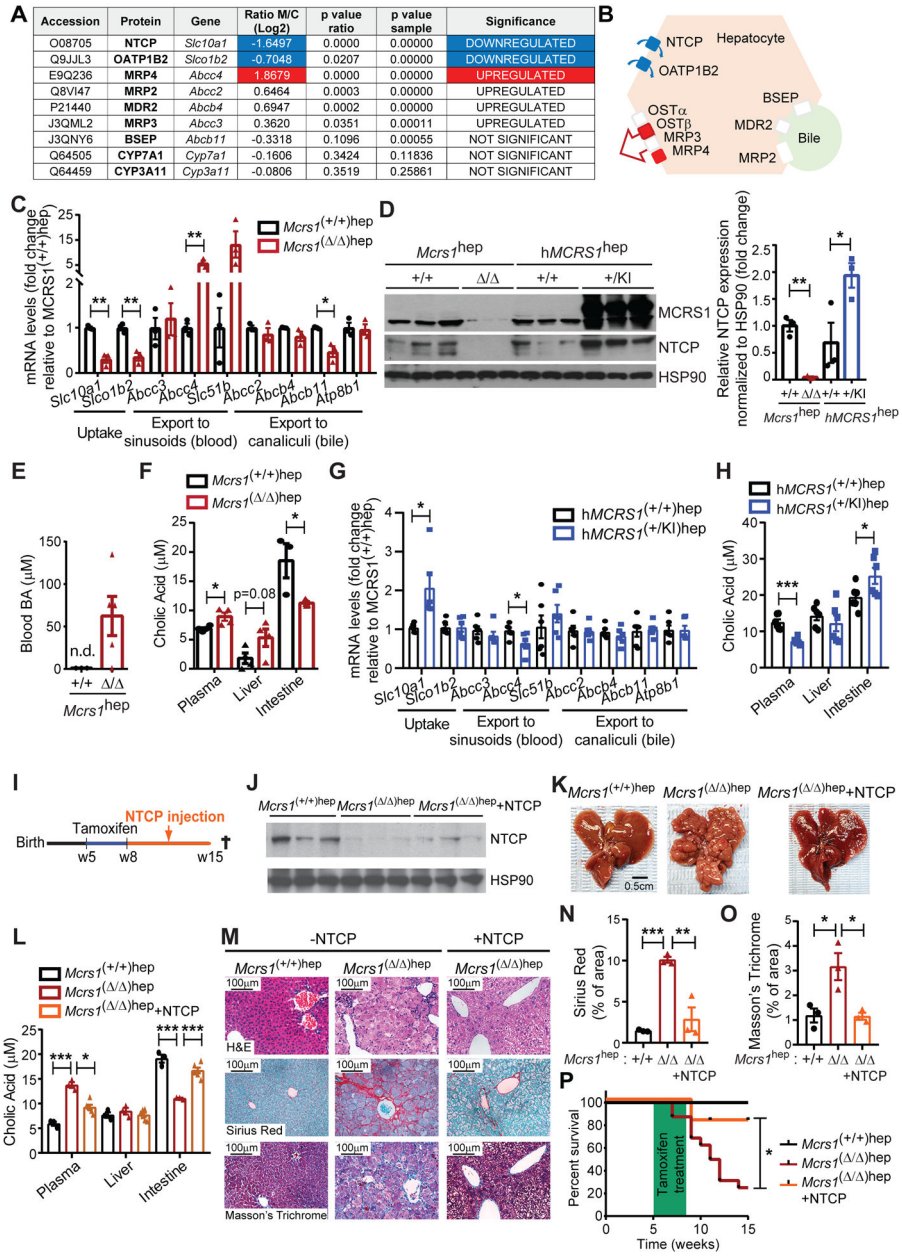

Accession	Protein	Gene	Ratio M/C (Log2)	p value ratio	p value sample	Significance
O08705	**NTCP**	*Slc10a1*	-1.6497	0.0000	0.00000	DOWNREGULATED
Q9JJL3	**OATP1B2**	*Slco1b2*	-0.7048	0.0207	0.00000	DOWNREGULATED
E9Q236	**MRP4**	*Abcc4*	1.8679	0.0000	0.00000	UPREGULATED
Q8VI47	**MRP2**	*Abcc2*	0.6464	0.0003	0.00000	UPREGULATED
P21440	**MDR2**	*Abcb4*	0.6947	0.0002	0.00000	UPREGULATED
J3QML2	**MRP3**	*Abcc3*	0.3620	0.0351	0.00011	UPREGULATED
J3QNY6	**BSEP**	*Abcb11*	-0.3318	0.1096	0.00055	NOT SIGNIFICANT
Q64505	**CYP7A1**	*Cyp7a1*	-0.1606	0.3424	0.11836	NOT SIGNIFICANT
Q64459	**CYP3A11**	*Cyp3a11*	-0.0806	0.3519	0.25861	NOT SIGNIFICANT

Fig. 2. Expression of BA transporters is deregulated in cirrhotic livers.

(A) Table representing relative BA-related protein levels detected by iTRAQ in livers from 8-week-old *Mcrs1*$^{(\Delta/\Delta)hep}$ mice compared to *Mcrs1*$^{(+/+)hep}$ mice (n=4). (B) Schematic representation of the location and expression status of BA transporters in the hepatocyte. Red means upregulated and green means downregulated. (C) Relative mRNA levels of BA transporters of hepatocytes isolated from 8-week-old *Mcrs1*$^{(+/+)hep}$ and *Mcrs1*$^{(\Delta/\Delta)hep}$ mice (n=3). (D) WB of isolated hepatocytes from 8-week-old *Mcrs1*$^{(+/+)hep}$, *Mcrs1*$^{(\Delta/\Delta)hep}$, *hMCRS1*$^{(+/+)hep}$ and *hMCRS1*$^{(+/KI)hep}$ mice. (E) Blood BA levels from 8-week-old *Mcrs1*$^{(+/+)hep}$ and *Mcrs1*$^{(\Delta/\Delta)hep}$ mice (n=3,5). (F) Cholic acid levels in plasma (n=4), liver (n=4) and intestine (n=3,5) from 8-week-old *Mcrs1*$^{(+/+)hep}$ and *Mcrs1*$^{(\Delta/\Delta)hep}$ mice. (G) Relative mRNA levels of BA transporters of hepatocytes isolated from 8-week-old

hMCRS1$^{(+/+)hep}$ and *hMCRS1*$^{(+/KI)hep}$ mice (n=6). (H) Cholic acid levels in plasma, liver and intestine from 8-week-old *hMCRS1*$^{(+/+)hep}$ and *hMCRS1*$^{(+/KI)hep}$ mice (n=6). (I) Schematic representation of 5-week-old NTCP-overexpressing *Mcrs1*^{hep} mice. (J) WB of isolated hepatocytes from the mice described in (I). (K) Representative pictures of livers from the mice described in (I). (L) Cholic acid levels in plasma, liver and intestine from mice described in (I) (n=3,3,6). (M) Representative pictures of indicated stainings of livers from mice described in (I). (N) and (O) Quantification of Sirius Red (N) and Masson's Trichrome (O) stainings described in (M) (n=3). (P) Survival of mice described in (I) (n=5,16,11). Scale bar: 0.5 cm in (K), and 100 μm in (M). Statistical analysis was performed using unpaired two-tailed Student's t test in (C), (D) and (F) to (H), two-way ANOVA with Tukey's multiple comparisons test in (L), (N) and (O), and Mantel-Cox test in (P). n.d. means not detected. Data are represented as means±SEM. *, $p \leq 0.05$; **, $p \leq 0.01$; ***, $p \leq 0.001$.

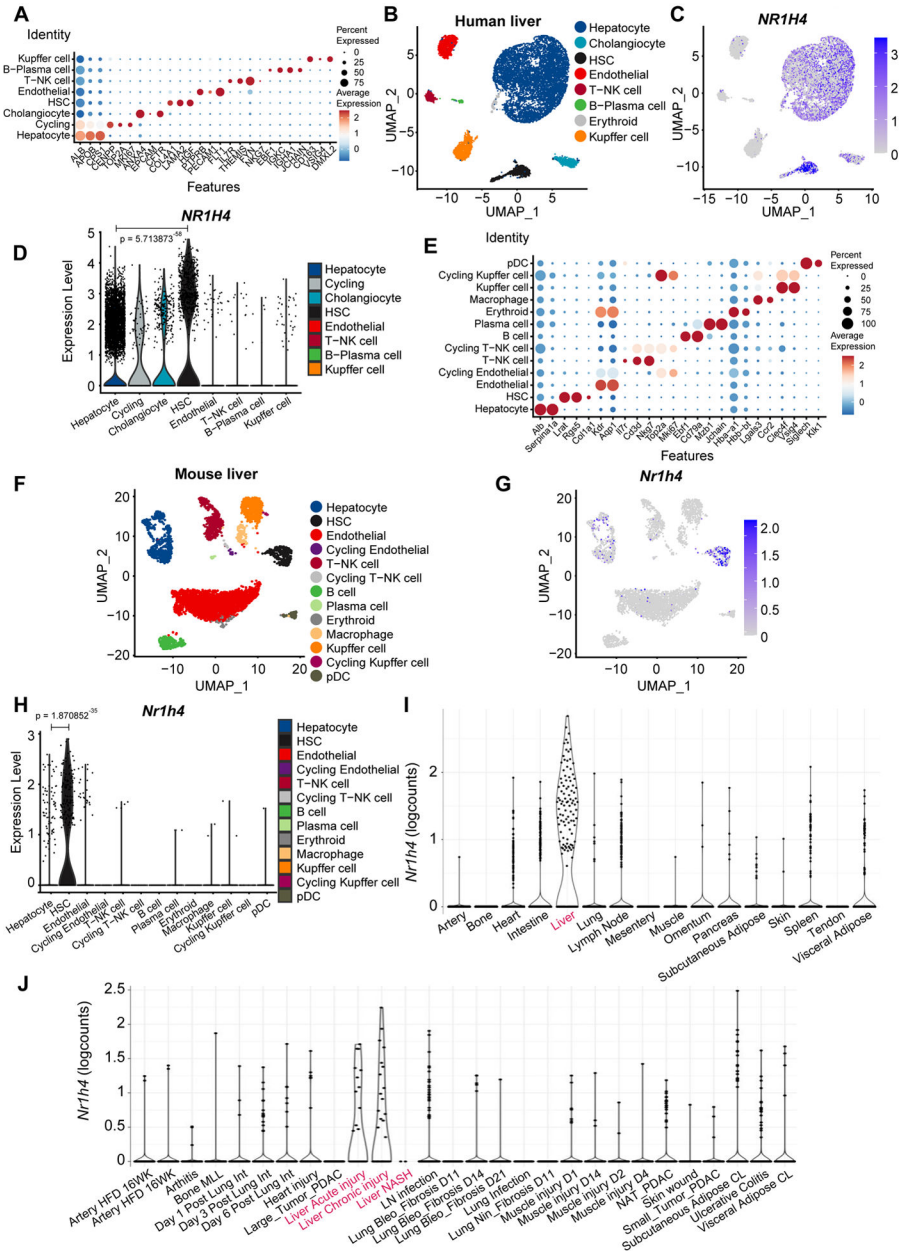

Fig. 3. FXR predominantly labels human and mouse HSCs.

(A) Annotation of cell types and selected marker genes obtained from single nuclei RNA sequencing (snRNA-seq) performed in human livers. Dot size indicates fraction of cells and colour indicates expression level (log-normalized and scaled). (B) Major clusters and respective cell-type assignments in UMAP from the experiment described in (A). (C) RNA expression of *NR1H4* in the same embedding as (B). (D) Violin plot representing gene expression levels of *NR1H4* from the experiment described in (A). (E) Annotation of cell types and selected marker genes obtained from single cell RNA sequencing (scRNA-seq) performed in liver tissue from healthy mouse. Dot size indicates fraction of cells and colour indicates expression level (log-normalized and scaled). (F) Major clusters and respective cell-type assignments in UMAP from the experiment described in (E). (G) RNA expression

of *Nr1h4* in the same embedding as (F). (H) Violin plot representing gene expression levels of *Nr1h4* from the experiment described in (E). (I) RNA expression of *Nr1h4* in fibroblasts from different tissues in steady-state mice. (J) RNA expression of *Nr1h4* in fibroblasts from disease mouse models. Statistical analysis was performed using the Wilcoxon rank sum test with continuity correction.

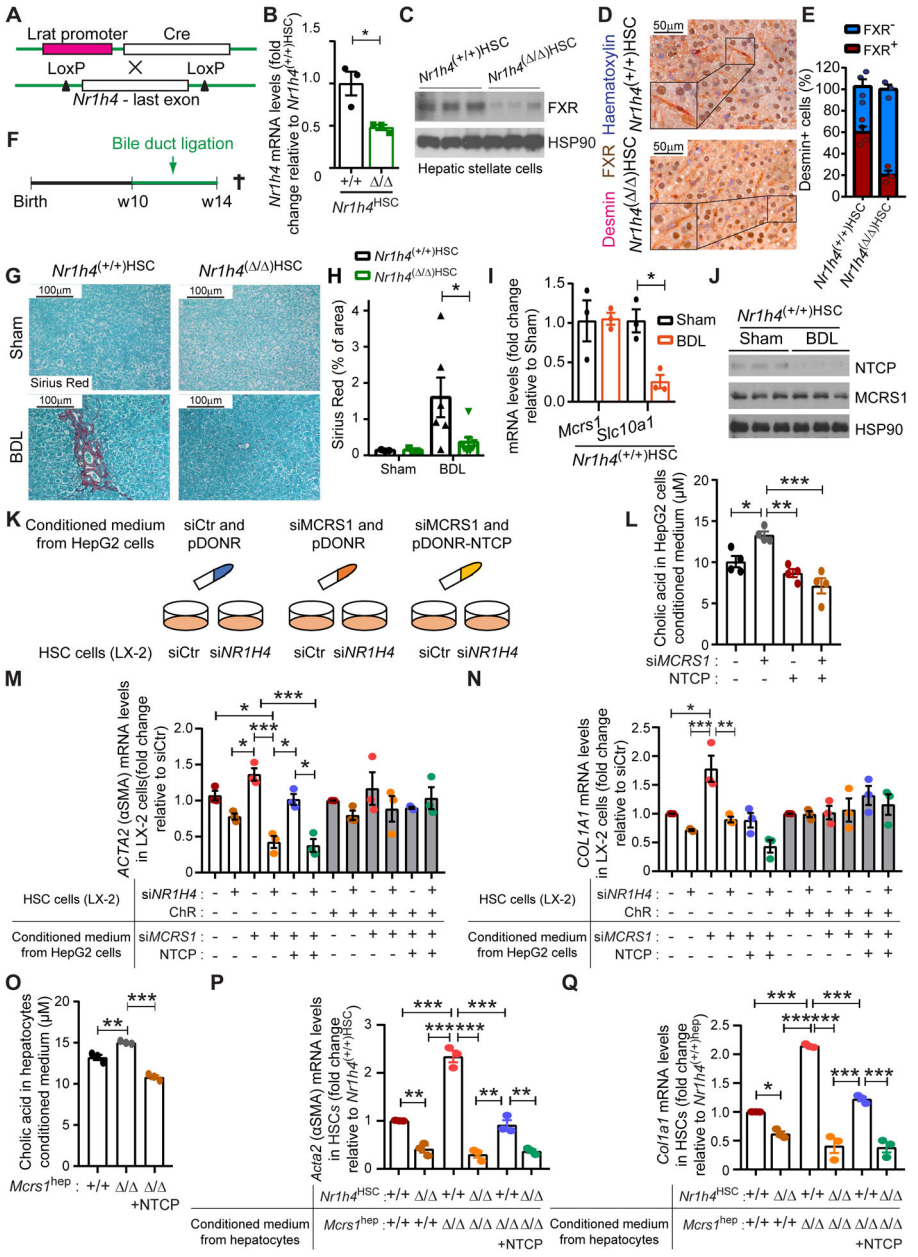

Fig. 4. BAs activate FXR in HSCs to promote liver fibrosis.

(A) Schematic representation of the *Nr1h4*^{HSC} mouse model. (B) Relative mRNA levels of *Nr1h4* of isolated HSCs from 14-week-old *Nr1h4*$^{(+/+)HSC}$ and *Nr1h4*$^{(\Delta/\Delta)HSC}$ mice (n=3). (C) WB of isolated HSCs from 14-week-old *Nr1h4*$^{(+/+)HSC}$ and *Nr1h4*$^{(\Delta/\Delta)HSC}$ mice. (D) Representative pictures of desmin/FXR co-IHC of livers from 14-week-old *Nr1h4*$^{(+/+)HSC}$ and *Nr1h4*$^{(\Delta/\Delta)HSC}$ mice. (E) Quantification of desmin/FXR co-IHC described in (D) (n=4,3). (F) Schematic representation of the bile duct ligation surgery protocol. (G) Representative pictures of Sirius Red staining of livers from 14-week-old *Nr1h4*$^{(+/+)HSC}$ and *Nr1h4*$^{(\Delta/\Delta)HSC}$ mice sham and bile duct-ligated (BDL). (H) Quantification of Sirius Red staining described in (G) (n=3,3,6,8). (I) Relative mRNA levels of indicated genes of isolated hepatocytes from *Nr1h4*$^{(+/+)HSC}$ mice sham and BDL (n=3). (J) WB of isolated

hepatocytes from *Nr1h4*$^{(+/+)HSC}$ mice sham and BDL. (K) Schematic representation of the *in vitro* experiment performed in HepG2 and LX-2 cell lines. (L) Cholic acid levels measured in media from HepG2 cells transfected with siCtr or si*MCRS1* and/or NTCP overexpression plasmid as indicated (N=4). (M) Relative mRNA levels of *ACTA2* in LX-2 cells transfected with siCtr or si*NR1H4* and treated with/without ChR, supplemented with conditioned medium from HepG2 cells transfected with siCtr or si*MCRS1* and pDONR-Ctr or pDONR-NTCP as indicated (N=3). (N) Relative mRNA levels of *COL1A1* in LX-2 cells transfected with siCtr or si*NR1H4* and treated with/without ChR, supplemented with conditioned medium from HepG2 cells transfected with siCtr or si*MCRS1* and pDONR-Ctr or pDONR-NTCP as indicated (N=3). (O) Cholic acid levels measured in media from isolated hepatocytes from *Mcrs1*^{hep} mice and *Mcrs1*$^{(\Delta/\Delta)hep}$ mice overexpressing NTCP (N=3). (P) Relative mRNA levels of *Acta2* in isolated HSCs from *Nr1h4*^{HSC} mice supplemented with conditioned medium from isolated hepatocytes from *Mcrs1*^{hep} mice and *Mcrs1*$^{(\Delta/\Delta)hep}$ mice overexpressing NTCP (N=3). (Q) Relative mRNA levels of *Col1a1* in isolated HSCs from *Nr1h4*^{HSC} mice supplemented with conditioned medium from isolated hepatocytes from *Mcrs1*^{hep} mice and *Mcrs1*$^{(\Delta/\Delta)hep}$ mice overexpressing NTCP (N=3). Scale bar: 50 μm in (D) and 100 μm in (G). Statistical analysis was performed using unpaired two-tailed Student's t test in (B) and (I), and two-way ANOVA with Tukey's multiple comparisons test in (H), and (L) to (Q). Data are represented as means±SEM. *, $p \leq 0.05$; **, $p \leq 0.01$; ***, $p \leq 0.001$.

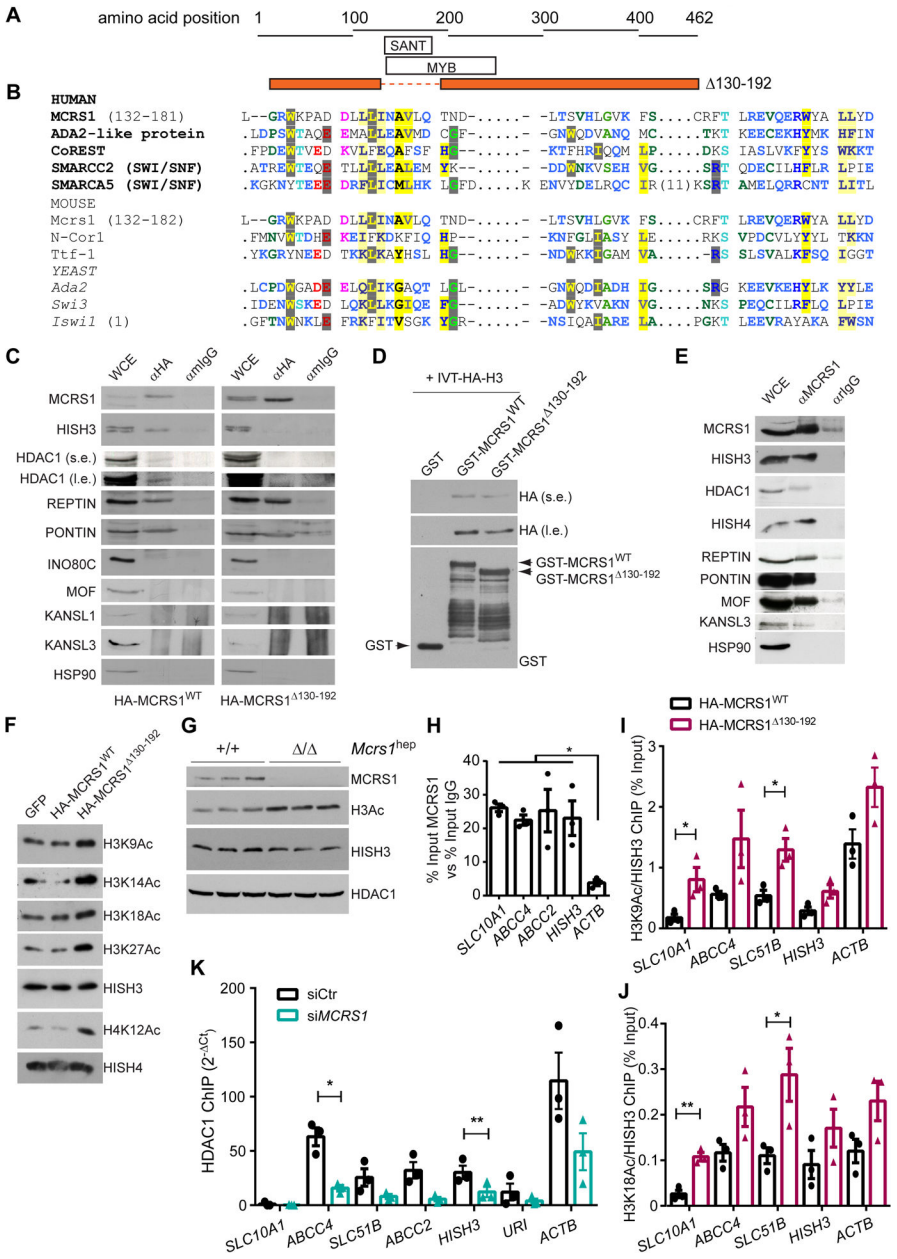

Fig. 5. MCRS1 regulates histone acetylation of BA transporter genes.

(A) Schematic representation of the protein sequence of MCRS1$^{\Delta 139–192}$ mutant. (B) Sequence alignment of human, mouse and yeast MCRS1 protein sequence with proteins containing a SANT domain. (C) IP performed in HepG2 cells overexpressing HA-MCRS1^{WT} and HA-MCRS1$^{\Delta 130–192}$ mutant proteins (N=3). s.e. and l.e. mean short exposure and long exposure, respectively. (D) WB performed in preparations of *in vitro* translated HA-HISH3 incubated with GST-, GST-MCRS1^{WT} and GST-MCRS1$^{\Delta 130–192}$. (E) IP performed in HepG2 cells (N=3). (F) WB of indicated proteins of core histones isolated from HepG2 cells overexpressing GFP, HA-MCRS1^{WT} and HA-MCRS1$^{\Delta 130–192}$ mutant proteins (N=3). (G) WB performed in isolated hepatocytes from 6-week-old *Mcrs1*$^{(+/+)hep}$ and *Mcrs1*$^{(\Delta/\Delta)hep}$ mice. (H) Chromatin IP (ChIP) using MCRS1 antibody performed in

HepG2 cells (N=3). (I) and (J) ChIPs using H3K9Ac (I) and H3K18Ac (J) antibodies performed in HepG2 cells overexpressing HA-MCRS1^{WT} and HA-MCRS1$^{\Delta 130–192}$ mutant proteins (N=3). (K) ChIP using HDAC1 antibody performed in HepG2 cells transfected with siCtr or si*MCRS1* (N=3). Statistical analysis was performed using two-way ANOVA with Tukey's multiple comparisons test in (H), and unpaired two-tailed Student's t test in (I) to (K). Data are represented as means±SEM. *, p≤0.05; **, p≤0.01.